



Cite this: Dalton Trans., 2020, **49**,
2129

UV-Vis-NIR absorption spectra of lanthanide oxides and fluorides†

Marcin Runowski, * Natalia Stopikowska and Stefan Lis

The absorption characteristics of lanthanide-based functional materials are of key importance for many scientists and engineers, *e.g.* in luminescence studies, bioimaging, optical heating/cooling, Raman spectroscopy, and industrial applications such as new light sources, optical sensors, labeling and tracing techniques, *etc.* Here we show the absorption spectra of solid, optically active lanthanide fluorides (CeF_3 , PrF_3 , NdF_3 , SmF_3 , EuF_3 , GdF_3 , TbF_3 , DyF_3 , HoF_3 , ErF_3 , TmF_3 , and YbF_3) and oxides (CeO_2 , Pr_6O_{11} , Nd_2O_3 , Sm_2O_3 , Eu_2O_3 , Gd_2O_3 , Tb_4O_7 , Dy_2O_3 , Ho_2O_3 , Er_2O_3 , Tm_2O_3 , and Yb_2O_3), measured in the UV-Vis-NIR range, from 200 to 2500 nm. The spectra were measured in diffused-reflectance mode using a spherical integrator. We assigned energy levels (${}^{2S+1}L_J$) of lanthanide ions(III), *i.e.* intraconfigurational 4f–4f transitions to the observed absorption bands. In order to clearly distinguish the 4f → 4f transitions, we also pointed out other absorption bands commonly observed in the measured spectra, such as intrinsic absorption of the matrices, interconfigurational 4f → 5d and charge transfer transitions, artificial bands from absorbed water (present in most materials) and a quartz holder.

Received 30th December 2019,
Accepted 22nd January 2020

DOI: 10.1039/c9dt04921e

rsc.li/dalton

Introduction

Compounds containing lanthanide (Ln) ions, mainly in the +3 oxidation state (Ln^{3+}), have been extensively studied both as liquid solutions and as solid materials, due to their favorable spectroscopic, magnetic and catalytic properties, which can be applied in both science and industry.^{1–19} All Ln elements can have a +3 oxidation state, which is usually their most stable configuration in various organic and inorganic matrices.^{11,20,21} However, lower +2 (*e.g.* Sm^{2+} and Eu^{2+}) and higher +4 (*e.g.* Ce^{4+} , Pr^{4+} and Tb^{4+}) oxidation states may also be stable and observable for some lanthanides in appropriate matrices and under a reducing or oxidizing atmosphere, respectively.^{11,20–22}

Systems based on Ln^{3+} possess unique spectroscopic properties, such as multicolor emission from the UV-Vis to NIR range, long luminescence lifetimes (μs –ms range) and narrow absorption/emission bands.^{11–26} These features are associated with several factors, such as: I) specific, ladder-like electronic structure of Ln^{3+} ; II) the forbidden character of the intrinsic 4f–4f transitions, governed by Laporte selection rules; III) crystal-field effects; and IV) the shielding of 4f electrons by 5s and 5p ones.^{12,20,21,27–29} Such remarkable and favorable spectroscopic

properties allow their wide range of applications as multicolor (UV-Vis-NIR) light sources, spectral converters for solar cells, and contactless temperature and pressure sensors, in advanced optoelectronics, in selective detection of various organic compounds and biological species, and in forensics for barcoding, tracing techniques, fingerprint detection, *etc.*^{6–10,14–16,22,26,30–38}

Ln^{3+} -doped inorganic particles such as bulk and nano-sized oxides, fluorides, borates, vanadates, phosphates, *etc.*, can be excited by UV light (200–400 nm) and can generate visible and NIR luminescence.^{15,22,26,28,37} Because the molar absorption coefficients of the forbidden 4f–4f transitions are relatively low, the emission of lanthanides is often enhanced by the use of energy transfer (from organic ligands or sensitizing ions, *e.g.* Ce^{3+}) and charge transfer (CT; usually from the oxygen anion present in the structure) processes.^{2,4–7,11–13,20,21,39} In contrast to organic compounds, they are resistant to photobleaching and high temperature treatment, and can also show efficient up-conversion emission, which is especially important for various biological applications, *e.g.* optical nanothermometry, imaging, luminescence detection, labeling, *etc.*^{11–18,22,26,37,38,40–43}

Finding the right excitation wavelength to measure the luminescence properties of a given system is a key issue. This is usually done by measuring the excitation or absorption spectra of the sample studied. However, because of technical reasons (*e.g.* availability of an NIR detector or appropriate light source), low signal intensity (low doping level), photodegradation of the sample, and so forth, such measurements may be hampered. Other problems in choosing the appropriate excitation wavelength (laser beam) may occur during Raman

Adam Mickiewicz University, Faculty of Chemistry, Department of Rare Earths, Uniwersytetu Poznańskiego 8, 61-614 Poznań, Poland. E-mail: runowski@amu.edu.pl ; Tel: +48 618291778

† Electronic supplementary information (ESI) available: Absorption spectra of lanthanide fluorides and oxides, as editable datasets in an Excel file; XRD data; spectra of water and quartz. See DOI: 10.1039/C9DT04921E

measurements. In such measurements, instead of the emission signal, Raman active modes are recorded, which are generally several orders of magnitude less intense than the luminescence signal. Therefore, when measuring Raman spectra, it is necessary to precisely select the laser whose wavelength does not match the absorption characteristics of the sample, which is very difficult in the case of Ln-doped compounds due to their very rich structure of energy levels.

Currently, the absorption spectra of all Ln^{3+} ions in aqueous solutions can be found in the work of Carnall.⁴⁴ However, there is no direct and explicit assignment of each band to a particular transition, *i.e.* energy level. In another work of Carnall *et al.*⁴⁵ centroids (in energy scale; cm^{-1}) for the energy levels of Ln^{3+} ions embedded (doped) in the LaF_3 host matrix can be found. However, in that paper the absorption spectra are provided only for Nd^{3+} -doped LaF_3 . Many scientists are currently investigating the optical properties of Ln-based inorganic bulk and nano-materials, many of which are fluorides, oxides or oxide-based materials (*e.g.* oxyfluorides, phosphates, vanadates, borates, *etc.*).^{26,31–38,40–42} Our intention was to collect in one paper absorption spectra for optically active Ln^{3+} ions embedded in typically studied inorganic fluoride and oxide matrices, and clearly assign the observed bands to individual transitions.

Here we present the absorption spectra of solid lanthanide fluorides and oxides, measured in diffused-reflectance mode, in the spectral range from ≈ 200 to 2500 nm. The observed absorption bands were assigned to the corresponding 4f–4f transitions in Ln^{3+} ions, and their centroids were determined in both wavelength (nm) and energy (cm^{-1}) scales. In this

work, we also focused on the determination of artifacts in spectra, *i.e.* absorption bands corresponding to water (absorbed by the samples), quartz (from the sample holder) and intrinsic absorption of matrices, which are often observed in the measured spectra, obscure their shape and may lead to the incorrect identification of the actual 4f–4f bands of optically active Ln^{3+} ions. For the convenience of readers, we provide direct access to the recorded spectra, *i.e.* editable data sets in Excel file, which can be found in the ESI.†

Experimental

Materials and synthesis

All the lanthanide oxides used (La_2O_3 , Pr_6O_{11} , Nd_2O_3 , Sm_2O_3 , Eu_2O_3 , Gd_2O_3 , Tb_4O_7 , Dy_2O_3 , Ho_2O_3 , Er_2O_3 , Tm_2O_3 , Yb_2O_3) were of 99.99% purity, and they were purchased from Stanford Materials (USA), except CeO_2 , which was synthesized from CeCl_3 (99.99%; Sigma Aldrich). Lanthanide fluorides (LnF_3) were prepared based on the appropriate chlorides (LnCl_3), obtained from the purchased lanthanide oxides. Detailed synthesis protocols and XRD data can be found in the ESI.†

Characterization

The UV-Vis-NIR absorption spectra of solid compounds were measured using a JASCO V-770 spectrophotometer, equipped with a spherical integrator ILN-925 (150 mm in diameter), two detectors, *i.e.* a photomultiplier in the UV-Vis range (200–850 nm) and a PbS detector in the NIR range

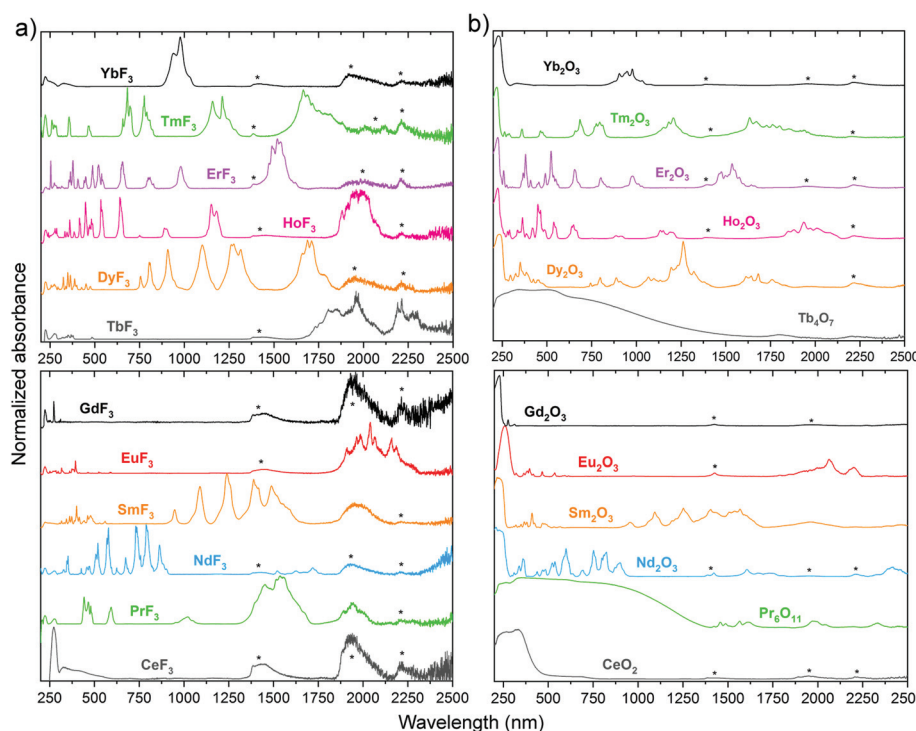


Fig. 1 Normalized absorption spectra of lanthanide fluorides (a) and oxides (b); asterisks indicate the bands corresponding to water and quartz absorption.

(850–2650 nm), and two light sources, *i.e.* deuterium (190–340 nm) and halogen lamps (340–2650 nm). The resolution in the UV-Vis range was 1 nm, and in the NIR range it was 4 nm (due to the lower sensitivity of the detector). X-ray powder diffraction (XRD) patterns were recorded using a Bruker AXS D8 Advance diffractometer in Bragg–Brentano geometry, with Cu K α 1 radiation ($\lambda = 1.5406 \text{ \AA}$), in the 2θ range from 6 to 60° , in 0.05° step scan mode.

Results and discussion

The spectra of Ln fluorides and oxides, *i.e.* LnF_3 and CeO_2 , Pr_6O_{11} , Nd_2O_3 , Sm_2O_3 , Eu_2O_3 , Gd_2O_3 , Tb_4O_7 , Dy_2O_3 , Ho_2O_3 , Er_2O_3 , Tm_2O_3 , Yb_2O_3 measured from 200 to 2500 nm, are presented in Fig. 1, and in the Excel file in the ESI† (editable datasets; up to 2600 and 2650 nm for $\text{Tb}^{3+}/4^+$ and Nd^{3+} compounds, respectively). They clearly show the relative intensities of the 4f–4f bands in the UV-Vis-NIR range and the 4f–5d and CT transitions, in relation to the absorption bands of the matrix and other artificial peaks, mainly originating from the absorbed water molecules and quartz holder. The magnified spectra for a single Ln ion in the series from Pr^{3+} to Yb^{3+} are shown in Fig. 2–12, emphasizing the forbidden, atomic-like 4f–4f transitions within the given Ln^{3+} . For better clarity, the spectra are presented in various ranges and are normalized to the most intense band observed in the presented range. For technical reasons, *i.e.* low sensitivity of the NIR detector above 2000 nm, only the spectra of Ln ions exhibiting a high absorption cross-section in the NIR range (a decent signal-to-noise ratio) are shown in this region in

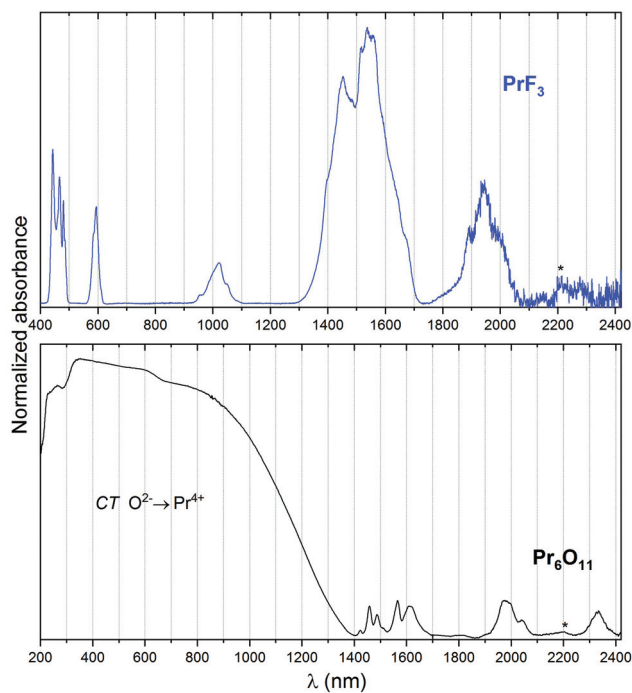


Fig. 2 Normalized absorption spectra of PrF_3 (blue) and Pr_6O_{11} (black).

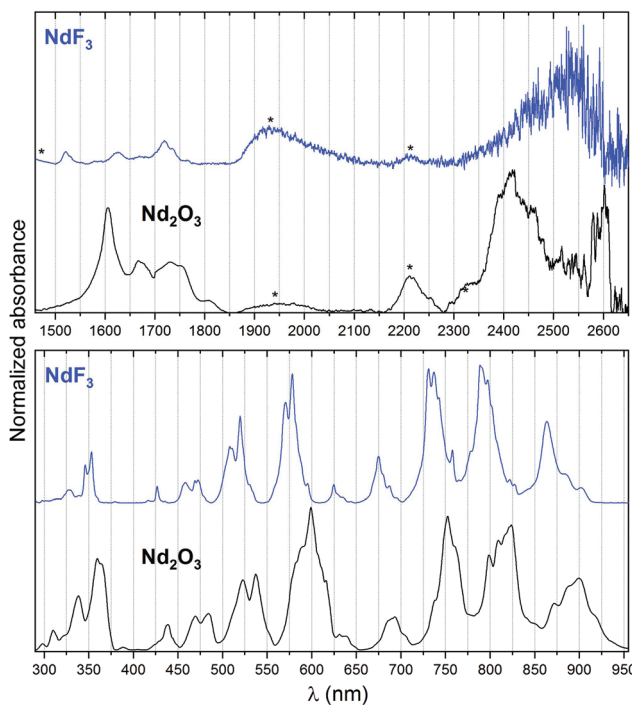


Fig. 3 Normalized absorption spectra of NdF_3 (blue) and Nd_2O_3 (black).

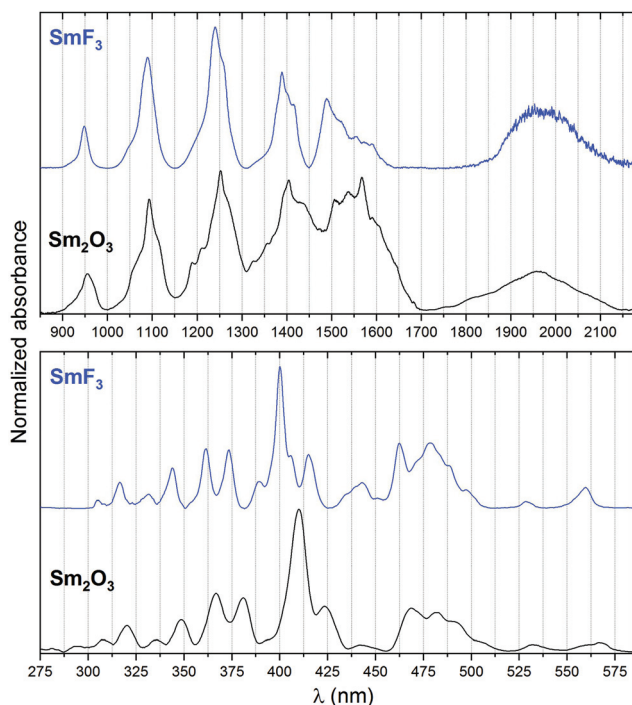


Fig. 4 Normalized absorption spectra of SmF_3 (blue) and Sm_2O_3 (black).

Fig. 2–12. The spectra of most of the oxides are magnified above 250–270 nm, due to the very high absorption of the oxide matrices in the far-UV, in comparison with the less intense 4f–4f transitions.

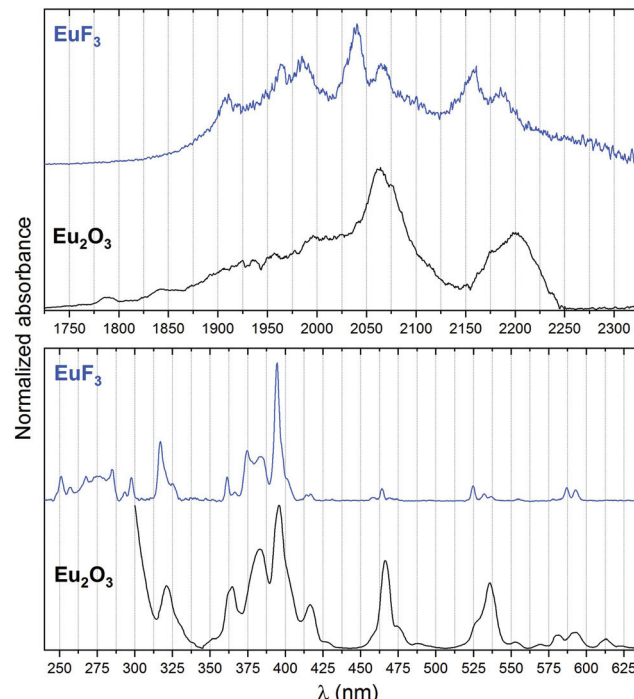


Fig. 5 Normalized absorption spectra of EuF_3 (blue) and Eu_2O_3 (black).

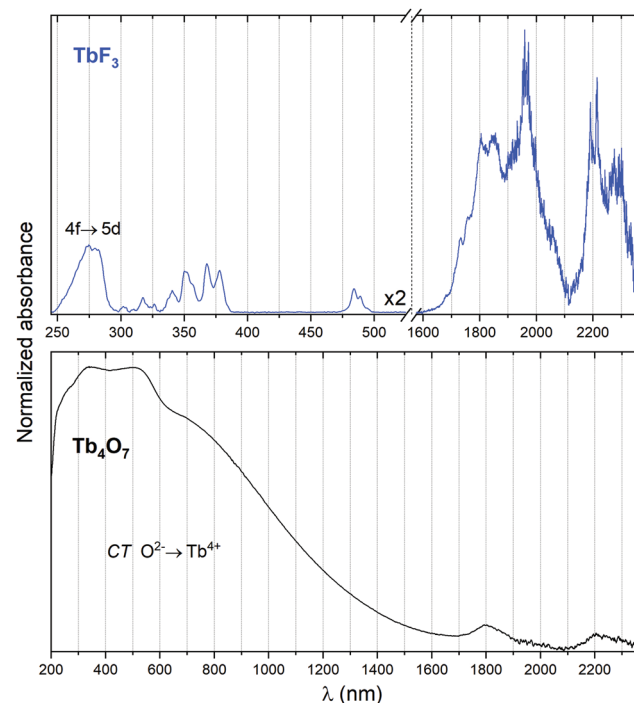


Fig. 7 Normalized absorption spectra of TbF_3 (blue) and Tb_4O_7 (black).

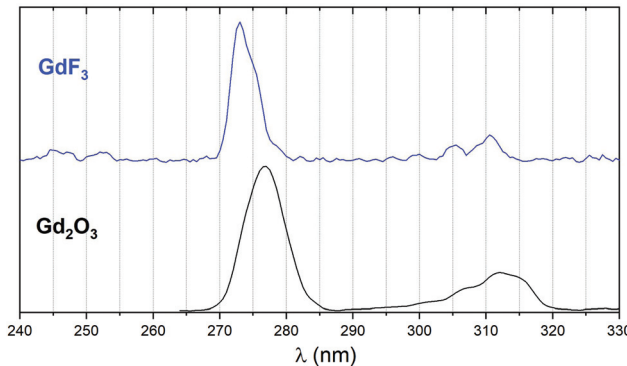


Fig. 6 Normalized absorption spectra of GdF_3 (blue) and Gd_2O_3 (black).

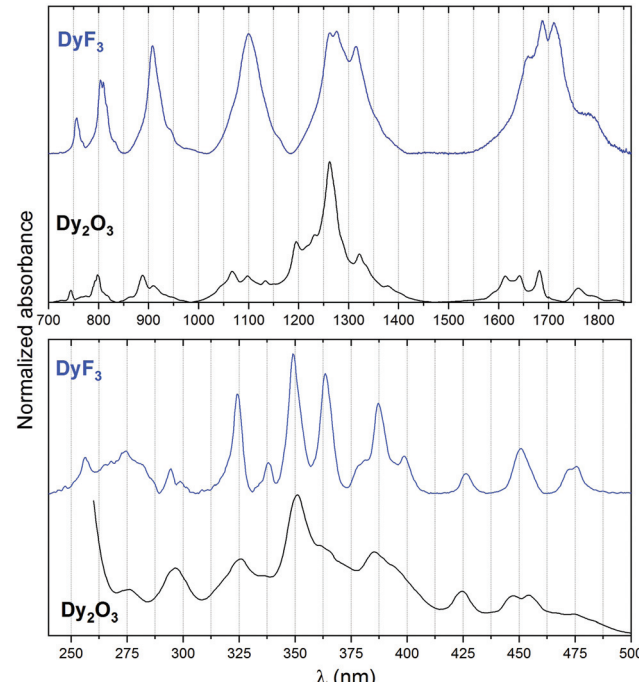


Fig. 8 Normalized absorption spectra of DyF_3 (blue) and Dy_2O_3 (black).

It is worth noting that the spectra of fluorides reveal two additional peaks around ≈ 224 and 275 nm (Fig. 1a), and the spectra of oxides have one very intense and broad, additional band around ≈ 230 nm (Fig. 1b). These bands are plausibly related to the absorption of the fluoride and oxide matrices, respectively, as they can be found in all compounds studied, including even in the optically inactive LaF_3 and La_2O_3 used as references, because La^{3+} has no 4f electrons (see the absorption spectra of LaF_3 and La_2O_3 in Fig. S2 in the ESI[†]). Depending on the amount of water absorbed by the sample (how hygroscopic the material is) and the intensity of the intra-configurational 4f–4f transitions in a particular Ln^{3+} ion, the relative intensities of the artificial broad bands (indicated by an asterisk) associated with the absorption of water at ≈ 1434

and 1934 nm, and quartz at ≈ 1385 and 2212 nm vary among the materials (see the absorption spectra of water and quartz in Fig. S3 and S4, respectively, in the ESI[†]). It should be remembered that the negative absorption (below the baseline/

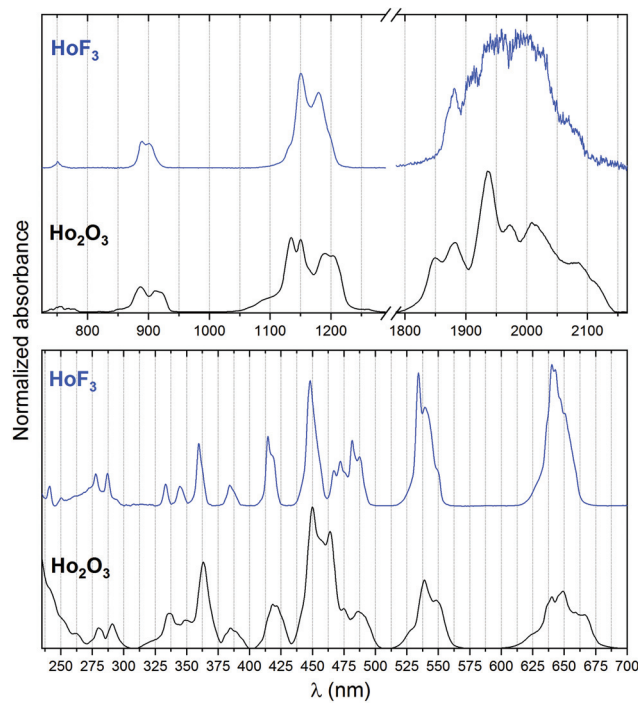


Fig. 9 Normalized absorption spectra of HoF_3 (blue) and Ho_2O_3 (black).

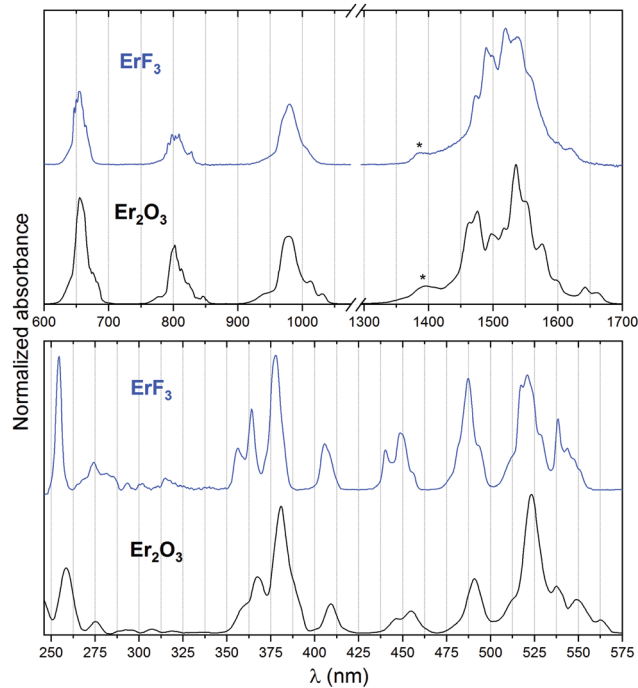


Fig. 10 Normalized absorption spectra of ErF_3 (blue) and Er_2O_3 (black).

noise level) observed for most of the fluorides, around ≈ 200 nm, is caused by the luminescence of Ln^{3+} ions (more light reaches the detector compared to the reference beam).

In all fluorides studied, Ln ions occur in the +3 oxidation state, whereas in the case of oxides the situation is more

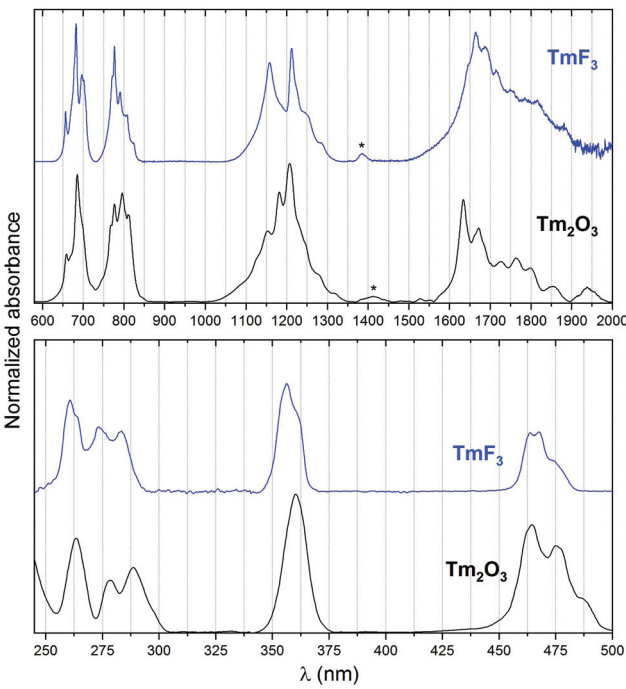


Fig. 11 Normalized absorption spectra of TmF_3 (blue) and Tm_2O_3 (black).

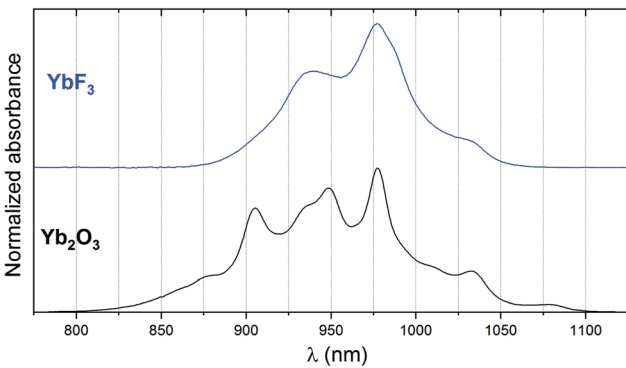


Fig. 12 Normalized absorption spectra of YbF_3 (blue) and Yb_2O_3 (black).

complex due to the stable +4 oxidation state in commercially available CeO_2 , Pr_6O_{11} ($\text{Pr}_2\text{O}_3 \cdot 4\text{PrO}_2$) and Tb_4O_7 ($\text{Tb}_2\text{O}_3 \cdot 2\text{TbO}_2$). Therefore, these three oxides exhibit very broad absorption bands corresponding to the allowed CT transitions, from oxygen to lanthanide ($\text{O}^{2-} \rightarrow \text{Ln}^{4+}$), *i.e.* CeO_2 from ≤ 200 to ≈ 750 nm; Pr_6O_{11} from ≤ 200 to ≈ 1400 nm; Tb_4O_7 from ≤ 200 to ≈ 1700 nm. The spectra of CeF_3 and TbF_3 show the broad bands corresponding to the allowed, interconfigurational $4f \rightarrow 5d$ ($4f^n \rightarrow 4f^{n-1}5d^1$) transitions, characteristic of Ce^{3+} and Tb^{3+} , *i.e.* CeF_3 from ≈ 200 to 310 nm; TbF_3 from ≈ 250 to 300 nm. The low intense, long “tail” of the absorption band observed from 300 to 600 nm in the spectrum of CeF_3 is plausibly associated with a small amount of the oxidized Ce^{4+} ions in the system (CT transition).

Table 1 Determined centroids for absorption bands corresponding to the 4f–4f transitions of Ln^{3+} , from ground to different excited states (${}^{2S+1}L_J$), given in wavelength (nm) and energy (cm $^{-1}$) scales

Excited state (${}^{2S+1}L_J$)	Wavelength (λ ; nm)		Wavenumber (energy; cm $^{-1}$)		Excited state (${}^{2S+1}L_J$)	Wavelength (λ ; nm)		Wavenumber (energy; cm $^{-1}$)	
	Oxide	LnF ₃	Oxide	LnF ₃		Oxide	LnF ₃	Oxide	LnF ₃
$\text{Pr}^{3+} {}^3\text{H}_4 \rightarrow {}^{2S+1}L_J$									
${}^3\text{H}_6$	2331	2280	4290	4386	${}^1\text{D}_2$	—	591	—	16 920
${}^3\text{F}_2$	1983	1945	5042	5141	${}^3\text{P}_0$	—	479.5	—	20 855
${}^3\text{F}_3$	1595	1542	6270	6485	${}^3\text{P}_1$	—	466	—	21 459
${}^3\text{F}_4$	1471	1430	6798	6993	${}^3\text{P}_2$	—	442	—	22 624
${}^1\text{G}_4$	—	1015	—	9852					
$\text{Nd}^{3+} {}^4\text{I}_{9/2} \rightarrow {}^{2S+1}L_J$									
${}^4\text{I}_{13/2}$	2463	2451	4060	4080	${}^4\text{G}_{9/2}$	522.5	509	19 138	19 646
${}^4\text{I}_{15/2}$	1736	1721	5760	5811	${}^2\text{D}_{3/2}$	484	471	20 661	21 231
	1669	1626	5992	6150	${}^4\text{G}_{11/2}$	469.5	458	21 299	21 834
	1606	1523	6227	6566	${}^2\text{P}_{1/2}$	438.5	426.5	22 805	23 446
${}^4\text{F}_{3/2}$	893	865	11 198	11 560	${}^2\text{D}_{5/2}$	427.5	416.5	23 391	24 010
${}^4\text{F}_{5/2}$	814	793.5	12 285	12 602	${}^2\text{P}_{3/2}$	388.5	379.5	25 740	26 350
${}^4\text{F}_{7/2}$	754	736.5	13 262	13 578	${}^4\text{D}_{1/2}, {}^4\text{D}_{3/2}, {}^4\text{D}_{5/2}$	361.5	353	27 662	28 328
							346		28 902
${}^4\text{F}_{9/2}$	690	675	14 492	14 814	${}^2\text{I}_{11/2}$	337	328	29 674	30 488
${}^2\text{H}_{11/2}$	633	624.5	15 797	16 012	?	309.5	—	32 310	—
${}^4\text{G}_{5/2}$	599	575.5	16 694	17 376	?	298	—	33 557	—
${}^4\text{G}_{7/2}$	537	520	18 621	19 230					
$\text{Sm}^{3+} {}^6\text{H}_{5/2} \rightarrow {}^{2S+1}L_J$									
${}^6\text{H}_{13/2}$	1963	1975	5094	5063	${}^4\text{M}_{17/2}$	443	443	22 573	22 573
${}^6\text{F}_{1/2}$	1567	1556	6381	6427	${}^4\text{G}_{9/2}$	442	439	22 624	22 779
${}^6\text{F}_{3/2}$	1537	1522	6506	6570	${}^4\text{I}_{15/2}$	434.5	—	23 015	23 015
${}^6\text{H}_{15/2}$	1507	1489	6636	6716	${}^6\text{P}_{5/2}$	423.5	415	23 613	24 096
${}^6\text{F}_{5/2}$	1404	1389	7122	7199	${}^4\text{L}_{13/2}$	406	—	24 630	24 630
${}^6\text{F}_{7/2}$	1252	1240	7987	8064	${}^4\text{F}_{7/2}$	410	400	24 390	25 000
${}^6\text{F}_{9/2}$	1093	1089	9149	9183	${}^4\text{L}_{15/2}$	389	—	25 707	25 707
${}^6\text{F}_{11/2}$	955	948	10 471	10 548	${}^6\text{P}_{7/2}$	381	373.5	26 246	26 774
${}^4\text{G}_{5/2}$	567	560	17 637	17 857	${}^4\text{D}_{3/2}$	366.5	361.5	27 285	27 662
${}^4\text{F}_{3/2}$	532	528	18 797	18 939	${}^4\text{D}_{7/2}$	348.5	344	28 694	29 070
${}^4\text{G}_{7/2}$	506	497.5	19 763	20 100	${}^4\text{H}_{11/2}$	336	332	29 762	30 120
${}^4\text{I}_{9/2}$	492	488.5	20 325	20 471	${}^2\text{K}_{15/2}$	320	316.5	31 250	31 595
${}^4\text{M}_{15/2}$	482	478.5	20 747	20 899	${}^4\text{G}_{9/2}$	308	305	32 467	32 786
${}^4\text{I}_{11/2}$	473	471.5	21 141	21 209	${}^2\text{K}_{13/2}$	295	—	33 898	—
${}^4\text{I}_{13/2}$	469	462.5	21 322	21 622	${}^2\text{N}_{19/2}$	281	—	35 587	—
${}^4\text{F}_{5/2}$	—	451	—	22 173					
$\text{Eu}^{3+} {}^7\text{F}_0 \rightarrow {}^{2S+1}L_J$									
${}^7\text{F}_6$	2049	2072	4880	4826	${}^5\text{D}_4$	361.5	361	27 662	27 701
${}^5\text{D}_0$	588.5	589.5	16 992	16 963	${}^5\text{H}_7$	329	325	30 769	30 395
${}^5\text{D}_1$	535	528	18 692	18 939	${}^5\text{H}_6$	321	317	31 546	31 152
${}^5\text{D}_2$	466.5	464	21 436	21 551	${}^5\text{F}_4$	—	297.5	—	33 613
${}^5\text{D}_3$	416.5	415.5	24 010	24 067	${}^5\text{I}_4$	—	293	—	34 129
${}^5\text{L}_6$	396	394.5	25 252	25 348	${}^5\text{I}_6$	—	285	—	35 088
${}^5\text{L}_7, {}^5\text{G}_2$	383	383.5	26 110	26 076	${}^5\text{K}_6$	—	267.5	—	37 383
${}^5\text{G}_{3-6}$	—	374	—	26 737	${}^3\text{K}_6$	—	256	—	39 062
${}^5\text{L}_8$	365	366.5	27 397	27 285	${}^3\text{D}_3$	—	251	—	39 840
$\text{Gd}^{3+} {}^8\text{S}_{7/2} \rightarrow {}^{2S+1}L_J$									
${}^6\text{P}_{7/2}$	313.5	310.5	31 898	32 206	${}^6\text{I}_{17/2}$	—	273	—	36 630
${}^6\text{P}_{5/2}$	306.5	305.5	32 626	32 733	${}^6\text{I}_{15/2}$	—	272	—	36 765
${}^6\text{P}_{3/2}$	304	300	32 895	33 333	${}^6\text{D}_{9/2}$	—	251	—	39 841
${}^6\text{I}_{7/2}$	—	278	—	35 971	${}^6\text{D}_{7/2}$	—	245	—	40 816
${}^6\text{I}_{9/2}$	277	275	36 101	36 364					
$\text{Tb}^{3+} {}^7\text{F}_6 \rightarrow {}^{2S+1}L_J$									
${}^7\text{F}_3$	2234	2240	4476	4464	${}^5\text{L}_9$	349	—	28 653	28 653
${}^7\text{F}_2$	—	1960	—	5102	${}^5\text{G}_3$	345	—	28 986	28 986
${}^7\text{F}_1$	1790	1790	5586	5586	${}^5\text{L}_8$	340	—	29 412	29 412
${}^7\text{F}_0$	—	1733	—	5770	${}^5\text{L}_7$	337	—	29 674	29 674
${}^5\text{D}_4$	—	486	—	20 576	${}^5\text{L}_6$	336	—	29 762	29 762
${}^5\text{D}_3$	—	384	—	26 041	${}^5\text{D}_1$	326	—	30 675	30 675
${}^5\text{G}_6$	—	375	—	26 667	${}^5\text{D}_0$	318	—	31 447	31 447
${}^5\text{L}_{10}$	—	369	—	27 100	${}^5\text{H}_7$	317	—	31 546	31 546
${}^5\text{G}_5$	—	357	—	28 011	${}^5\text{H}_6$	302	—	33 113	33 113
${}^5\text{D}_2$	—	352	—	28 409					
$\text{Dy}^{3+} {}^6\text{H}_{15/2} \rightarrow {}^{2S+1}L_J$									
${}^6\text{H}_{11/2}$	1678	1694	5959	5903	${}^4\text{M}_{21/2}$	399	399	25 063	25 063
${}^6\text{H}_{9/2}, {}^6\text{F}_{11/2}$	1262	1287	7924	7770	${}^4\text{I}_{13/2}, {}^4\text{F}_{7/2}, {}^4\text{K}_{17/2}$	385	387.5	25 974	25 806

Table 1 (Contd.)

Excited state ($^{2S+1}L_J$)	Wavelength (λ ; nm)		Wavenumber (energy; cm^{-1})		Excited state ($^{2S+1}L_J$)	Wavelength (λ ; nm)		Wavenumber (energy; cm^{-1})	
	Oxide	LnF_3	Oxide	LnF_3		Oxide	LnF_3	Oxide	LnF_3
$^6\text{F}_{9/2}$	1095	1101	9132	9083	$^4\text{M}_{19/2}$	—	380	—	26 316
$^6\text{F}_{7/2}$	895	909	11 173	11 001	$^4\text{I}_{11/2}$	364	364	27 473	27 473
$^6\text{F}_{5/2}$	797	807	12 547	12 392	$^6\text{P}_{7/2}, ^4\text{M}_{15/2}$	352	350	28 409	28 571
$^6\text{F}_{3/2}$	744	756.5	13 440	13 219	$^4\text{F}_{5/2}$	—	338	—	29 586
$^6\text{F}_{1/2}$	725	724.5	13 793	13 803	$^6\text{P}_{3/2}, ^4\text{K}_{15/2}$	326	324.5	30 675	30 817
$^4\text{F}_{9/2}$	474	474	21 097	21 097	$^4\text{H}_{11/2}, ^4\text{G}_{9/2}$	296	295	33 784	33 898
$^4\text{H}_{15/2}$	452	451	22 124	22 173	$^4\text{L}_{17/2}$	276	273	36 232	36 630
$^4\text{G}_{11/2}$	425	426.5	23 529	23 447	$^4\text{K}_{11/2}$	—	256.5	—	38 986
$\text{Ho}^{3+} \text{I}_8 \rightarrow {}^{2S+1}L_J$									
$^5\text{I}_7$	1967	1972	5084	5071	$^5\text{G}_4$	388.5	387.5	25 740	25 806
$^5\text{I}_6$	1164	1165	8591	8584	$^3\text{K}_7$	385.5	385	25 940	25 974
$^5\text{I}_5$	900	896	11 111	11 161	$^3\text{H}_6$	363	360	27 548	27 778
$^5\text{I}_4$	758	751	13 193	13 316	$^5\text{G}_3$	350	345	28 571	28 986
$^5\text{F}_5$	648.5	644	15 420	15 528	$^5\text{G}_2$	335	333	29 851	30 030
$^5\text{S}_2$	551.5	539	18 132	18 553	$^3\text{M}_{10}$	—	294	—	34 014
$^5\text{F}_4$	539.5	534	18 536	18 727	$^5\text{D}_4$	291	287	34 364	34 843
$^5\text{F}_3$	487.5	483.5	20 513	20 683	$^3\text{G}_3$	280	278	35 714	35 971
$^5\text{F}_2$	476	472.5	21 008	21 164	$^3\text{H}_5$	274.5	272	—	36 765
$^3\text{K}_8$	463.5	467	21 575	21 413	$^3\text{I}_7, ^3\text{F}_4$	263	261	38 023	38 314
$^5\text{G}_6$	450.5	449	22 198	22 272	?	??253	250	39 526	40 000
$^5\text{G}_5$	420	416.5	23 810	24 010	?	243	241	41 152	41 580
$\text{Er}^{3+} \text{I}_{15/2} \rightarrow {}^{2S+1}L_J$									
$^4\text{I}_{13/2}$	1520	1521	6579	6575	$^2\text{H}_{9/2}$	409	407	24 450	24 559
$^4\text{I}_{11/2}$	980	980	10 204	10 204	$^4\text{G}_{11/2}$	381	377.5	26 247	26 490
$^4\text{I}_{9/2}$	804	804.5	12 438	12 430	$^2\text{G}_{9/2}$	367.5	364	27 211	27 472
$^4\text{F}_{9/2}$	657	654.5	15 221	15 278	$^2\text{G}_{7/2}$	359	356.5	27 855	28 050
$^4\text{S}_{3/2}$	549	542	18 215	18 446	$^2\text{P}_{3/2}$	320.5	317	31 201	31 546
$^2\text{H}_{11/2}$	523.5	521	19 102	19 192	$^2\text{K}_{13/2}$	307	302	32 573	33 113
$^4\text{F}_{7/2}$	491	487	20 366	20 538	$^2\text{D}_{7/2}$	294	293.5	34 014	34 072
$^4\text{F}_{5/2}$	455	449	21 978	22 259	$^4\text{G}_{9/2}$	275.5	274.5	36 298	36 430
$^4\text{F}_{3/2}$	446.5	440.5	22 396	22 706	$^4\text{D}_{7/2}$	258.5	254.5	38 685	39 293
$\text{Tm}^{3+} \text{H}_6 \rightarrow {}^{2S+1}L_J$									
$^3\text{F}_4$	1719	1729	5817	5784	$^1\text{D}_2$	360	357	27 778	28 011
$^3\text{H}_5$	1192	1192	8389	8389	$^3\text{P}_0$	289	283	34 602	35 336
$^3\text{H}_4$	789	787.5	12 674	12 698	$^3\text{P}_1$	278.5	274	35 907	36 496
$^3\text{F}_3$	688.5	687	14 524	14 556	$^1\text{I}_6$	—	264.5	—	37 807
$^3\text{F}_2$	659	657	15 174	15 221	$^3\text{P}_2$	264	260.5	37 879	38 388
$^1\text{G}_4$	469	467	21 321	21 413					
$\text{Yb}^{3+} \text{F}_{7/2} \rightarrow {}^{2S+1}L_J$									
$^2\text{F}_{5/2}$	951	971.5	10 515	10 293					

We determined centroids in the wavelength (nm) and energy (cm^{-1}) scales for the observed absorption bands of Ln^{3+} , associated with intraconfigurational 4f–4f transitions from their ground to different excited states, up to around 40 000 cm^{-1} (see Table 1). The energy levels of Ln^{3+} ions were assigned based on the studies of Carnall *et al.*^{44,45} and van der Ende *et al.*,⁴⁶ in the commonly used notation ${}^{2S+1}L_J$ where S is the total spin quantum number, L is the total orbital quantum number and J is the total angular momentum quantum number.

In general, the absorption bands of lanthanide oxides are slightly red-shifted toward a larger wavelength compared to the corresponding fluorides (see Fig. 2–12), for example, the 4f–4f transitions of all Ln^{3+} ions (except of Dy^{3+}) in the Ln_2O_3 have systematically lower energies than the corresponding transitions in the LnF_3 matrices. This is due to the crystal-field effects (the nephelauxetic effect), *i.e.* the stronger overlapping of the bonding orbitals between the Ln^{3+} ions and the ligands

(O^{2-} and F^-), leading to a higher covalency (shorter bonds) in the lanthanide fluorides than that in the corresponding oxides. Moreover, most of the absorption bands in LnF_3 are narrower than the corresponding bands in Ln_2O_3 , due to the different coordination environments around the Ln^{3+} ions in these matrices. It is noteworthy that the relative intensity ratios of the bands corresponding to the same 4f–4f transitions are different for fluoride and oxide matrices. This effect can be particularly well observed, *e.g.* in the case of EuF_3 and Eu_2O_3 (visible range), and for DyF_3 and Dy_2O_3 (NIR range).

Conclusions

We provide an extensive comparison of the absorption spectra of solids (powders), lanthanide fluorides and oxides, *i.e.* LnF_3 and CeO_2 , Pr_6O_{11} , Nd_2O_3 , Sm_2O_3 , Eu_2O_3 , Gd_2O_3 , Tb_2O_7 , Dy_2O_3 , Ho_2O_3 , Er_2O_3 , Tm_2O_3 , Yb_2O_3 , recorded in a wide UV-Vis-NIR

spectral range, from 200 to \approx 2500 nm. Particular attention was paid to the absorption bands corresponding to the 4f–4f transitions, which were magnified in order to clearly present the spectral ranges in which individual Ln^{3+} ions are optically active. The peak centroids determined for the observed 4f–4f bands, in both fluoride and oxide matrices, are compared and presented in Table 1. For the convenience of readers, we also provide the recorded spectra in the form of editable datasets (Excel file†). To facilitate the unambiguous assignment of the Ln^{3+} 4f–4f transitions in the spectra, we have clearly indicated and discussed commonly observed additional bands in the spectra, corresponding to the matrix absorption, $4f \rightarrow 5d$ and CT transitions, and the absorption of water and quartz. This spectral database can act as a comprehensive reference source for many scientists and engineers dealing with lanthanide-based functional materials, *e.g.* their use in spectroscopy, optics, sensing techniques, lighting applications, bioimaging, forensics, *etc.*

Conflicts of interest

The authors declare no conflict of interest.

Acknowledgements

This work was supported by the Polish National Science Centre (grant no. 2016/21/B/ST5/00110).

References

- 1 J.-C. G. Bünzli and I. McGill, *Ullmann's Encyclopedia of Industrial Chemistry*, Wiley-VCH Verlag GmbH & Co. KGaA, Weinheim, Germany, 2018, pp. 1–53.
- 2 S. Ogata, T. Shimizu, T. Ishibashi, Y. Ishiyone, M. Hanami, M. Ito, A. Ishii, S. Kawaguchi, K. Sugimoto and M. Hasegawa, *New J. Chem.*, 2017, **41**, 6385–6394.
- 3 J. Xu, T. M. Corneillie, E. G. Moore, G.-L. Law, N. G. Butlin and K. N. Raymond, *J. Am. Chem. Soc.*, 2011, **133**, 19900–19910.
- 4 X. Qin, X. Liu, W. Huang, M. Bettinelli and X. Liu, *Chem. Rev.*, 2017, **117**, 4488–4527.
- 5 K.-L. Wong, G.-L. Law, Y.-Y. Yang and W.-T. Wong, *Adv. Mater.*, 2006, **18**, 1051–1054.
- 6 J. Lucas, P. Lucas, T. Le Mercier, A. Rollat and W. Davenport, *Rare Earths*, Elsevier, 2015, pp. 319–332.
- 7 G.-L. Law, K.-L. Wong, H.-L. Tam, K.-W. Cheah and W.-T. Wong, *Inorg. Chem.*, 2009, **48**, 10492–10494.
- 8 J. Xu, A. Gulzar, P. Yang, H. Bi, D. Yang, S. Gai, F. He, J. Lin, B. Xing and D. Jin, *Coord. Chem. Rev.*, 2019, **381**, 104–134.
- 9 U. Cho, D. P. Riordan, P. Cieplak, K. S. Kocherlakota, J. K. Chen and P. B. Harbury, *Nat. Chem. Biol.*, 2018, **14**, 15–21.
- 10 J. Zhou, J. L. Leaño, Z. Liu, D. Jin, K.-L. Wong, R.-S. Liu and J.-C. G. Bünzli, *Small*, 2018, **14**, 1801882.
- 11 K. Binnemans, *Chem. Rev.*, 2009, **109**, 4283–4374.
- 12 S. Lis, *J. Alloys Compd.*, 2002, **341**, 45–50.
- 13 J.-C. G. Bünzli, *Coord. Chem. Rev.*, 2015, **293–294**, 19–47.
- 14 C. D. S. Brites, A. Millán and L. D. Carlos, *Handbook on the Physics and Chemistry of Rare Earths*, 2016, vol. 49, pp. 339–427.
- 15 M. Runowski, A. Shylichuk, A. Tymiński, T. Grzyb, V. Lavín and S. Lis, *ACS Appl. Mater. Interfaces*, 2018, **10**, 17269–17279.
- 16 J. Reszczyńska, T. Grzyb, J. W. Sobczak, W. Lisowski, M. Gazda, B. Ohtani and A. Zaleska, *Appl. Catal., B*, 2015, **163**, 40–49.
- 17 A. Gnach and A. Bednarkiewicz, *Nano Today*, 2012, **7**, 532–563.
- 18 W. Zheng, P. Huang, D. Tu, E. Ma, H. Zhu and X. Chen, *Chem. Soc. Rev.*, 2015, **44**, 1379–1415.
- 19 G. Wang, Q. Peng and Y. Li, *Acc. Chem. Res.*, 2011, **44**, 322–332.
- 20 J.-C. G. Bünzli, *Trends Chem.*, 2019, **1**(8), P751–762.
- 21 B. G. Wybourne and L. Smentek, *Optical spectroscopy of lanthanides*, CRC Press, New York, 2007.
- 22 M. Runowski, P. Woźny, V. Lavín and S. Lis, *Sens. Actuators, B*, 2018, **273**, 585–591.
- 23 S. Cotton, *Lanthanide and Actinide Chemistry*, John Wiley & Sons, Ltd, Chichester, UK, 2006.
- 24 K. L. Bray, M. Glasbeek, H. Kunkely and A. Vogler, Transition Metal and Rare Earth Compounds, in *Excited States, Transitions, Interactions I*, ed. H. Yersin, Springer, New York, 2001.
- 25 V. S. Sastri, J.-C. Bünzli, V. R. Rao, G. V. S. Rayudu and J. R. Perumareddi, *Modern Aspects of Rare Earths and Their Complexes*, Elsevier, 2003.
- 26 M. Runowski, J. Marciniak, T. Grzyb, D. Przybylska, A. Shylichuk, B. Barszcz, A. Katrusiak and S. Lis, *Nanoscale*, 2017, **9**, 16030–16037.
- 27 O. L. Malta, *J. Non-Cryst. Solids*, 2008, **354**, 4770–4776.
- 28 A. Shylichuk, R. T. Moura, A. N. Carneiro Neto, M. Runowski, M. S. Zarad, A. Szczeszak, S. Lis and O. L. Malta, *J. Phys. Chem. C*, 2016, **120**, 28497–28508.
- 29 P. A. Tanner, *Chem. Soc. Rev.*, 2013, **42**, 5090–5101.
- 30 M. Runowski, N. Stopikowska, D. Szeremeta, S. Goderski, M. Skwierczyńska and S. Lis, *ACS Appl. Mater. Interfaces*, 2019, **11**, 13389–13396.
- 31 Q. Guo, C. Zhao, Z. Jiang, L. Liao, H. Liu, D. Yang and L. Mei, *Dyes Pigm.*, 2017, **139**, 361–371.
- 32 H. Ye, M. He, T. Zhou, Q. Guo, J. Zhang, L. Liao, L. Mei, H. Liu and M. Runowski, *J. Alloys Compd.*, 2018, **757**, 79–86.
- 33 P. Kumar, K. Nagpal and B. K. Gupta, *ACS Appl. Mater. Interfaces*, 2017, **9**, 14301–14308.
- 34 R. Ma, R. Shimmon, A. McDonagh, P. Maynard, C. Lennard and C. Roux, *Forensic Sci. Int.*, 2012, **217**, e23–e26.

- 35 M. Skwierczyńska, M. Runowski, S. Goderski, J. Szczytko, J. Rybusiński, P. Kulpiński and S. Lis, *ACS Omega*, 2018, **3**, 10383–10390.
- 36 L. Marciniak and A. Bednarkiewicz, *Sens. Actuators, B*, 2017, **243**, 388–393.
- 37 M. Runowski, P. Woźny, N. Stopikowska, Q. Guo and S. Lis, *ACS Appl. Mater. Interfaces*, 2019, **11**, 4131–4138.
- 38 C. Hazra, V. N. K. B. Adusumalli and V. Mahalingam, *ACS Appl. Mater. Interfaces*, 2014, **6**, 7833–7839.
- 39 A. K. R. Junker, L. R. Hill, A. L. Thompson, S. Faulkner and T. J. Sørensen, *Dalton Trans.*, 2018, **47**, 4794–4803.
- 40 A. Nadort, J. Zhao and E. M. Goldys, *Nanoscale*, 2016, **8**, 13099–13130.
- 41 Y. Liu, D. Tu, H. Zhu and X. Chen, *Chem. Soc. Rev.*, 2013, **42**, 6924–6958.
- 42 C. S. Lim, V. V. Atuchin, A. S. Aleksandrovsky, M. S. Molokeev and A. S. Oreshonkov, *J. Alloys Compd.*, 2017, **695**, 737–746.
- 43 C. I. Silva Filho, A. L. Oliveira, S. C. F. Pereira, G. F. de Sá, L. L. da Luz and S. Alves, *Dalton Trans.*, 2019, **48**, 2574–2581.
- 44 W. T. Carnall, *Handbook on the Physics and Chemistry of Rare Earths*, 1979, pp. 171–208.
- 45 W. T. Carnall, H. Crosswhite and H. M. Crosswhite, *Energy level structure and transition probabilities in the spectra of the trivalent lanthanides in LaF₃*, Argonne National Laboratory Report, Argonne, IL (United States), 1978.
- 46 B. M. van der Ende, L. Aarts and A. Meijerink, *Phys. Chem. Chem. Phys.*, 2009, **11**, 11081–11095.